Transient Surface Patterns and Instabilities at Adhesive Junctions of Viscoelastic Films

Hongbo Zeng,[†] Yu Tian,[†,‡] Boxin Zhao,[†] Matthew Tirrell,[†] and Jacob Israelachvili*[,†]

Department of Chemical Engineering, Materials Department, and Materials Research Laboratory, University of California, Santa Barbara, California 93106, and State Key Lab of Tribology, Department of Precision Instruments, Tsinghua University, Beijing 100084, China

Received June 8, 2007; Revised Manuscript Received August 14, 2007

ABSTRACT: A new kind of self-organized transient fingering pattern and instability was found to generally exist during the adhesive contact and coalescence of two polymer films in the viscous or viscoelastic state. The average radius of the patterns was found to increase with contact time following $r = (r_i + r_o)/2 \propto t^n$, where r_o and r_i are the outer and inner radii of the fingers, and where n varies from 0.15 to 0.3 depending on the viscoelastic properties of the materials. The surface approach rate has no effect on the appearance of the fingering patterns once it is less than some critical rate. The lifetime of the fingering patterns increases with the polymer viscosity as $\tau \propto \eta^n$ ($n = 1.6 \pm 0.2$), and peaks at some critical film thickness. The mechanism for the transient patterns is discussed in terms of theories of fluid mechanics and the molecular forces between surfaces.

Introduction

The contact and adhesion of two surfaces is a common phenomenon in nature and industry, and it is important for understanding adhesives, liquid−liquid coalescence, agglomeration and dispersal of colloidal particles, friction and lubrication, wear, and many other phenomena, including biological processes such as cell−cell coalescence and cell−substrate spreading.[1−3] Experimental and theoretical work on the "contact mechanics" and "adhesion mechanics" of surfaces has steadily progressed for more than 100 years, beginning with the pioneering work of Hertz[1,3] in 1882 on the deformations of two nonadhering elastic spheres when pressed into contact. In the Hertz theory, since there is no adhesion between the contacting spheres, the stresses are everywhere compressive and the spheres separate freely at zero load (zero adhesion force).[1,3]

In 1971, Johnson, Kendall, and Roberts extended the Hertz theory to include adhesion, i.e., taking into account the surface energies of the materials but neglecting the surface forces at finite surface separations.[4] The approximation of the Johnson−Kendall−Roberts (JKR) theory leads to a larger contact area (under a given load) than in the Hertz theory, and a finite tensile load (finite adhesion force) is required to separate the solids. However, the JKR equations, based on continuum elasticity theory, lead to infinite tensile stresses and strains at the contact boundary (because the finite surface forces are assumed to act over an infinitely small distance). To remove these singularities, Derjaguin, Muller, and Toporov (DMT) in 1975 proposed another theory that takes the surfaces forces outside the contact zone into account, but the DMT theory assumes that the profile of the deformed surfaces remains Hertzian.[5] The DMT model leads to adhesive (tensile) stresses that are finite outside the contact zone but zero inside, which results in a stress discontinuity at the edge of the contact zone. The DMT theory predicts an adhesion force of $F_{ad} = 2\pi RW$, while the JKR theory predicts $F_{ad} = (3/2)\pi RW$, where W is the work of adhesion per unit area, and R is the local radius of the surface approaching a flat surface (R is replaced by $R/2$ for two spheres of radius R). In 1977, Tabor compared the JKR and DMT theories and pointed out their main drawbacks.[6]

In 1980, abandoning the hypothesis of the original DMT theory, Muller et al.[7] carried out a self-consistent numerical calculation using a Lennard-Jones potential, and obtained a continuous transition of the adhesion force F_{ad} and profiles from the DMT to the JKR theory when a dimensionless parameter μ increases. This dimensionless parameter is proportional to the one introduced by Tabor in 1977 (the Tabor number[6]), which can be interpreted as the ratio of the range of the main elastic deformation (strain) to the effective range of surface forces (stress). The JKR theory is usually applicable to soft materials with large surface energies and radii ($\mu \gg 1$), and the DMT theory applies to small, rigid spheres (or asperities) with low surface energies ($\mu \ll 1$).

In 1992, a unified model for elastic contacts was proposed by Maugis,[8] based on the Dugdale model,[9] which assumes that the adhesion force acting outside the contact zone has a constant value over some critical distance. The Maugis model, called the *cohesive zone model*, provides an analytic relation between the air gap distance between the two surfaces and the normal stress resisting separation of the surfaces outside the contact zone. The Maugis model removes the singularity of the JKR theory, the stress discontinuity of the DMT theory, and also provides a connection between the elastic contact problem (contact mechanics) and linear elastic fracture mechanics.[10−13]

The above classic Hertz, JKR, DMT, and Maugis theories or models of "contact mechanics" describe the adhesion and deformations of two initially curved purely *elastic* materials. However, most real materials are viscoelastic, especially when considered over a large range of time scales or rates of interaction and also at high temperatures. Over the last 2 decades, research has focused on understanding the "contact dynamics" of viscoelastic materials, both theoretically and experimentally.[2,10−28] However, due to the complexity of the problem, even the simplest case of the contact of two linear viscoelastic spheres is still not completely understood. All the above classic contact mechanics models are static (equilibrium)

* Corresponding author. E-mail: jacob@engineering.ucsb.edu.
[†] Department of Chemical Engineering, Materials Department, and Materials Research Laboratory, University of California, Santa Barbara.
[‡] State Key Lab of Tribology, Department of Precision Instruments, Tsinghua University.

10.1021/ma0712807 CCC: $37.00
Published on Web 10/10/2007

Table 1. Measured Thin Film Shear Viscosities (Mean Values[a])

polymer (at 24 °C)	closest separation, D, and radius of gyration, R_g[29, 53, 54]	film viscosity η_{film} (Pa s)	bulk viscosity η_{bulk} (Pa s)
PBD	$D \approx 240$ nm, $R_g \approx 3$ nm	5 ± 2	6
PDMS 1	$D \approx 300$ nm, $R_g > 10$ nm	20 ± 5	30
PDMS 2	$D \approx 450$ nm, $R_g > 10$ nm	120 ± 10[b]	800[b]
PS 590	$D \approx 230$ nm, $R_g \approx 0.7$ nm	210 ± 30	230
PS 800	$D \approx 215$ nm, $R_g \approx 0.8$ nm	$2{,}900 \pm 200$	2800
PS 1390 at 60 °C	$D \approx 260$ nm, $R_g \approx 1.0$ nm	$(1.3 \pm 0.2) \times 10^5$	N/A

[a] Quoted "mean" values refer to the values averaged across the films of thickness D. [b] The atypically large difference in the two viscosities for this sample may be due to a small amount of solvent still remaining in the PDMS films even after overnight drying in vacuum.[46]

Table 2. Scaling Laws Obtained from the Experiments

	power law relationship	power law index
mean contact radius, r	$r = (r_i + r_o)/2 \propto t^n$	$n = 0.25 \pm 0.05$ for $\eta_{film} < 10^4$ Pa s; $n \approx 0.155 \pm 0.005$ for $\eta_{film} \geq 10^5$ Pa s
lifetime of the transient fingering patterns, τ	$\tau \propto \eta^n$	$n = 1.6 \pm 0.2$
wavelength of the fingers, λ	$\lambda \propto t^n$	$n = 0.25 \pm 0.05$ for $\eta_{film} < 10^4$ Pa s; $n \approx 0.155 \pm 0.005$ for $\eta_{film} \geq 10^5$ Pa s

models, describing the final *equilibrium* state for elastic materials, and appear to be unsuited for dealing with the *dynamic* growth of a fluid or viscoelastic contact junction after adhesive contact or "coalescence" has occurred, which is usually due both to molecular-scale intermixing across the contact interface and to bulk flow.

While there has been much work on fingering instabilities of confined films under tensile loading conditions (e.g., detaching or peeling surfaces, necking, cavitation, crack propagation and failure),[13,17,29−35] and some recent work on fingering patterns developed during crack closure (adhesion) of thin elastic solids,[36−42] the transients associated with adhesion of viscous (liquid-like), viscoelastic, and even elastic (solid-like), materials are still largely unknown although it is generally believed that there are no abrupt changes or esoteric surface shape transitions associated with the adhesion process. A detailed understanding of these transients is of fundamental interest in interface and surface science and of practical importance in many technological and biological processes.

Very recently, using a surface forces apparatus (SFA) and an optical interference technique employing fringes of equal chromatic order (FECO),[43,44] we have measured the dynamic surface deformations during (symmetric) polymer−polymer adhesion and coalescence, and the related phenomenon of (asymmetric) polymer−solid substrate adhesion and spreading.[45,46] Unlike the materials in the elastic state that obey the classical theories of contact mechanics, viscous liquid-like and viscoelastic materials appear to go through an early stage where highly ordered transient surface fingering patterns are observed during both symmetric coalescence and asymmetric spreading. After this initial phase the surface profiles are simple constant mean curvature necks.[45,46] The factors that determine the lifetime of the transient patterns (the time from the appearance of the fingers to their disappearance) are investigated in this study for a *symmetrical* system. In particular, we report and discuss the effects of the approach rate, the material viscosity, the film thickness, and their surface or interfacial energy. A possible mechanism to explain the observations is proposed, and the implications and potential applications of such transient phenomena are discussed.

Materials and Experimental Methods

Three different kinds of polymers were chosen for this study: polystyrene (PS), poly(dimethylsiloxane) (PDMS), and polybutadiene (PBD). Polystyrene $M_w = 1390$ (PS 1390), $M_w/M_n \leq 1.06$, $T_g \approx 46$ °C (measured by differential scanning calorimetry (DSC) at a heating rate of 10 °C/min) and polystyrene $M_w = 800$ (PS 800), $M_w/M_n \leq 1.3$, were purchased from Pressure Chemical Co.; PS 590, $M_w/M_n \leq 1.1$, was purchased from Scientific Polymer Products Inc.; PBD 7000, $M_w/M_n \leq 1.1$, and PDMS of two different viscosities (the molecular weights were not supplied by the suppliers) were purchased from Sigma-Aldrich and United Chemical Technologies (the bulk shear viscosities η_{bulk} and measured film viscosities η_{film} of the different polymers are shown in Table 1).

All polymers were used as received without further purification. The bulk shear viscosities η_{bulk} of the polymers used were measured using an ARES controlled strain rheometer from Rheometrics Scientific in a cone−plate geometry with 25 mm diameter plates and 0.1 rad cone angle at the experimental temperature of 24.0 ± 0.2 °C. The polymer film shear viscosities η_{film} were measured by rheological experiments using the SFA as previously described.[29,45,46]

The polymer films were prepared by spin-coating a droplet of polymer solution (PS in toluene, PBD in tetrahydrofuran, PDMS in hexane or tetrahydrofuran) on a mica substrate glued on silica disks, then very slowly drying under reduced pressure overnight (>10 h) to remove the solvent and leave a film of uniform thickness, then mounted into the SFA chamber. The film thickness T_0 could be controlled by changing the concentration of polymer solution (0.5−10 wt %) and the spin-coating speed (500−6000 rpm) to obtain uniform polymer films (of PS, PBD and PDMS) in the thickness range $T = 50$−5000 nm. Film thicknesses were measured in situ in the SFA using the FECO optical interference technique.[43,44]

An SFA Mark III[47] was used to study the fine details of the surface shape changes during the adhesion process. The two surfaces were mounted in the SFA chamber in the "crossed cylinders" geometry (each cylinder of radius $R = 2$ cm), which locally corresponds to a sphere of radius R on a flat surface or to two spheres of radius $2R$. The polymer surfaces were brought together using a motor-controlled micrometer at various speeds from 10 to 250 nm/s. Once closer than some critical distance (~10 nm, see ref 45), they jumped into adhesive contact due to the attractive van der Waals force between them. On impact, the curved surfaces immediately flatten quasi-elastically, i.e., with no or little flow, to a finite contact area due to the adhesion force pulling them together. This is followed by a slower but continuous "coalescence" involving the flow of the viscoelastic material across and around the contact junction (analogous to a "crack healing" process), increasing the contact area and changing the local surface geometry. All these changes were recorded for periods ranging from seconds to >10 h. The polymers used in this study have high viscosities that allowed for real time visualization and VCR recording of the surface deformations using both the FECO interference fringes and normal optical microscopy. The simultaneously recorded FECO fringes and top-view microscope images were later analyzed and compared to obtain the full picture at the nano- and microscales.

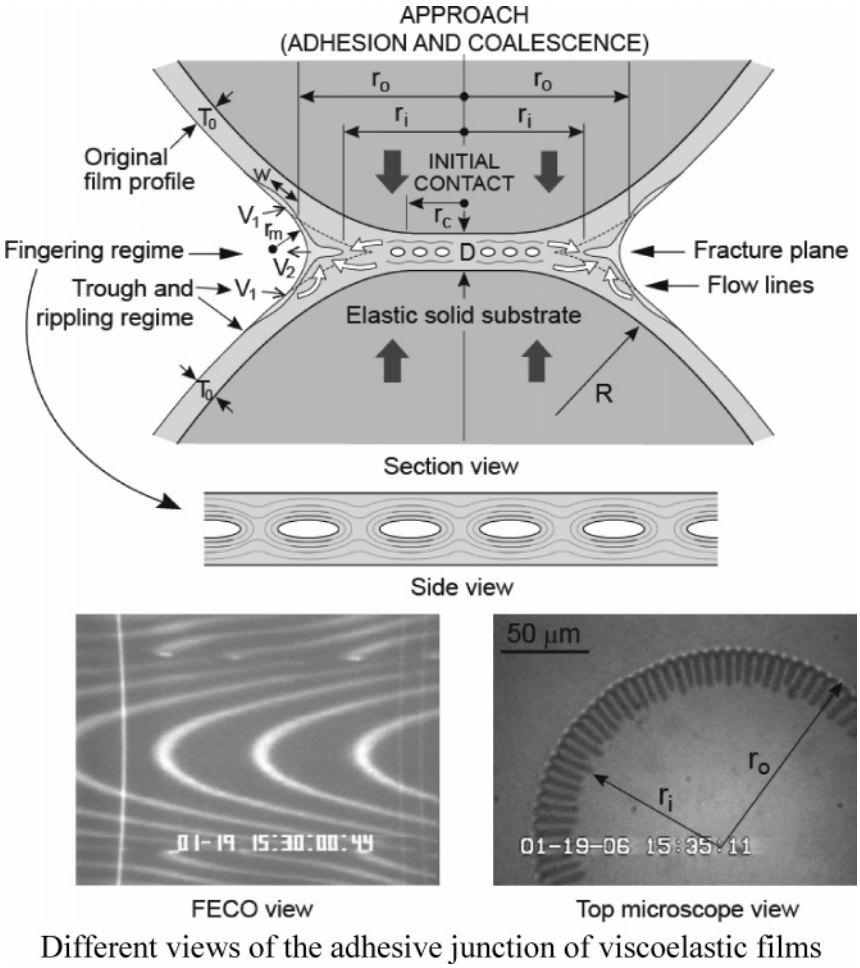

Figure 1. Schematics (top), FECO optical fringe (bottom, left), and normal optical microscope image (bottom, right) of contact geometry and transient fingering instabilities and capillary waves/ripples observed during the adhesion and coalescence of two viscous or viscoelastic films.

Most of the experiments in this study were performed at room temperature (24 °C) if not mentioned otherwise. Some experiments were performed at higher temperatures, up to 90 °C. The temperature of the SFA was increased by using two heating rods (100 W, 110 V), inserted into the metal walls of the SFA chamber, and the temperature inside was monitored using a thermistor.

The patterned adhesive junctions were preserved by using physical or chemical methods such as rapid quenching or UV cross-linking. For low molecular weight, low viscosity polymers, rapid quenching was found to be a good way to "fix" the patterns, as described as follows for PS 1390: Two PS 1390 films were brought into contact at a high-temperature (~80 °C where $\eta \approx 1000$ Pa s). At the point where a pattern was to be frozen, liquid nitrogen was injected into the SFA chamber. The two surfaces were then separated, and imaged using a FEI Sirion scanning electron microscope (SEM) from FEI Company, Hillsboro, OR, a Nikon OPTIPHOT 200 microscope, and an atomic force microscope (Dimension 3100 AFM) from Veeco Metrology, LLC, Santa Barbara, CA. This method is similar to that used previously to image the alignment of liquid alkane molecules in thin films between two shearing surfaces.[48] When required, imaging can be done at low temperatures, and it is also possible to chemically characterize the surfaces using X-ray photoelectron spectroscopy (XPS) or secondary ion mass spectroscopy (SIMS).[49,50]

Results, Analysis, and Discussion

I. Changes in the Contact Diameter and Confined Film Thickness with Time. The surfaces were brought together using a linear motor-driven micrometer. Once they were closer than some critical distance ($D \sim 10$ nm), they jump into adhesive contact due to the attractive van der Waals force between them. At this point the motor was stopped (approach velocity $v \rightarrow 0$). As previously reported,[46] a novel type of fingering pattern was observed to develop ahead of the growing contact circle (or neck) immediately after the jump into contact for all the polymer melts studied at room temperature. A schematic of the typical local geometry is shown in Figure 1, showing the different velocities of growth at different locations of the polymer surfaces during the transient "fingering stage" of the coalescence, where r_o and r_i are the outer and inner radii of the fingers at any instant time t for films of initial thickness T_0.

Figures 2 and 3 show the rates of growth of PS800 and PS590 films for different initial film thicknesses T_0. The outer and inner diameters, $2r_o$ and $2r_i$, were obtained from the FECO fringes (Figure 1, bottom left) and/or the top-view microscopic images (Figure 1, bottom right). For all the polymer melts studied (and at different initial film thicknesses), both the $2r_o$ and $2r_i$ were found to follow a power-law function of time t, although r_o was less well-defined than r_i. Initially, the two radii are the same, then they diverge, then the rate of growth of the outer radius slows down until the two merge, which defines the point at which the fingers disappear. Overall, based on the data shown in Figure 2, the average contact radius r shows a scaling relationship with time t of the form

$$r = (1/2)(r_i + r_o) = f(\rho, \gamma, R, \eta, T_0)t^n \propto t^n \qquad (1)$$

with $n = 0.2-0.3$, where $f(\rho, \gamma, R, \eta, T_0)$ is a function of the polymer density ρ, surface tension γ, viscosity η, initial film thickness T_0, and local substrate curvature R. When the polymer

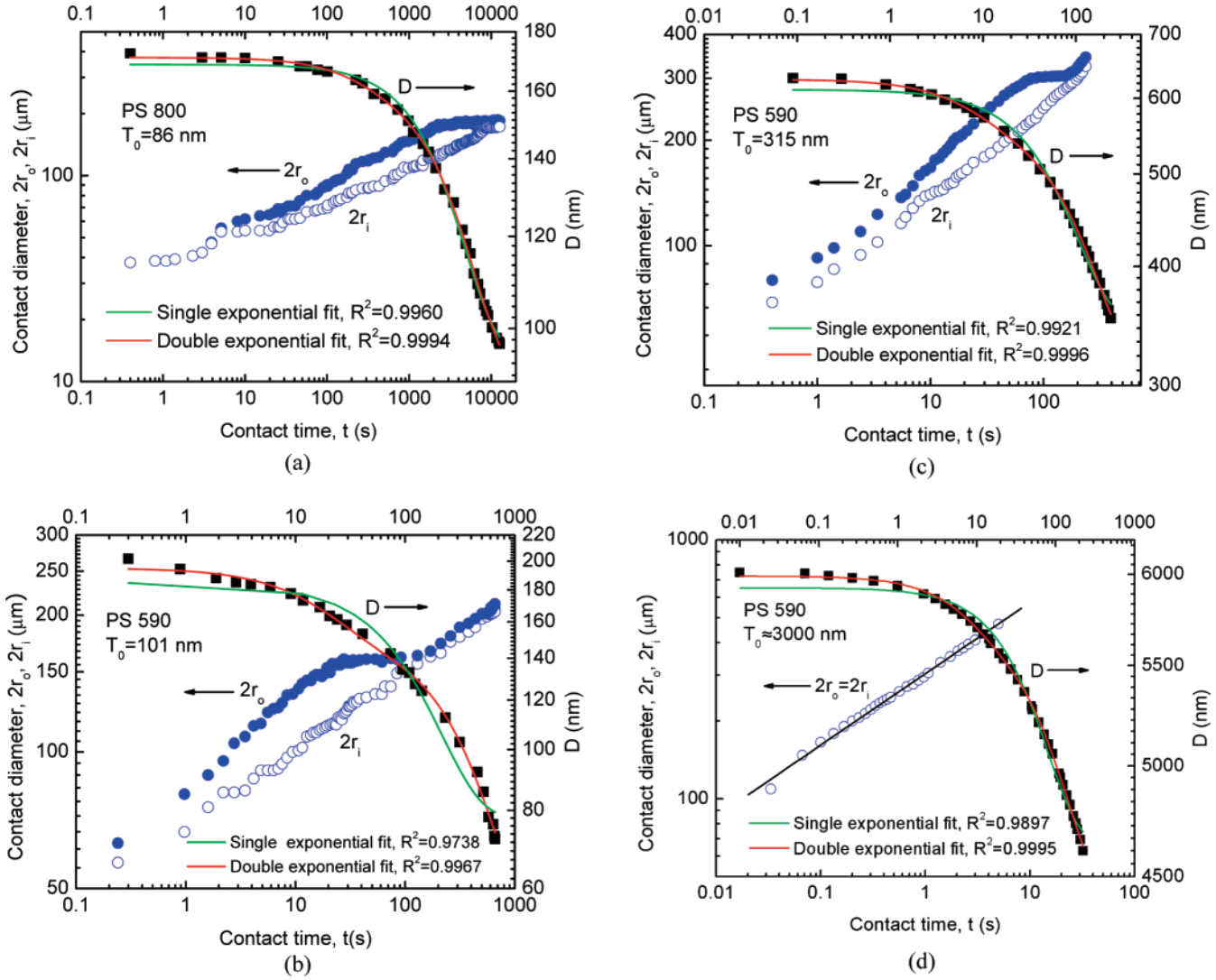

Figure 2. Outer and inner contact diameters and minimum gap distances D (as defined and shown in Figure 1), vs contact time t during the adhesive coalescence of different polymer films with different initial thicknesses, T_0. The bulk viscosities of PS 800 and PS 590 are 2800 and 230 Pa s, respectively.

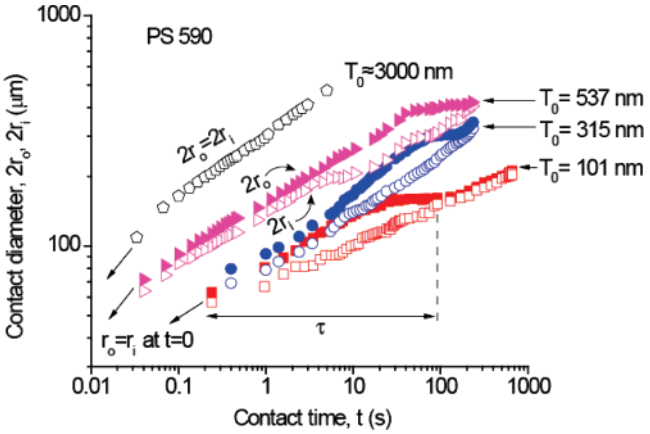

Figure 3. Cumulative results for the outer and inner contact diameters (as defined and shown in Figure 1) vs contact time t during the adhesive coalescence of two PS 590 films for four different initial thicknesses, T_0.

film thickness is greater than some critical value, cf. Figure 2d for PS 590 and $T_0 \approx 3\ \mu$m, only a featureless rounded neck is observed, whose radius r increases as $r \propto t^n$,with $n = 0.27 \pm 0.01$, i.e., about the same dependence as the mean value of $n = 0.2-0.3$ for finger growth.

Thus, the increasing of the contact neck radii with time appears to be independent of whether fingers are present or not, and is therefore representative of a more general phenomenon which has been studied before for smooth circular necks. Various theories have predicted a $r_o \propto t^n$ dependence, with n varying from 0.1 to 0.5 depending on whether the flow is due to the coalescence of two liquid droplets, when $n = 0.5$ (although a t ln t dependence has also been predicted by Eggers et al.[25]), or to the spreading of a liquid on a solid surface, when $n = 0.10-0.125$.[24,51] Our systems appear to belong somewhere in between these two regimes, i.e., involving liquids spreading on films of the same material but of finite thickness, hence the likely reason for the observed exponents ($n = 0.2-0.3$) falling between 0.1 and 0.5.

The changes of the minimum gap distance or total film thickness, D, defined in Figure 1, with time are also shown in Figure 2. The data follow a double exponential decay function better than a single exponential, as given by eq 2:

$$D = C_1 e^{-t/\tau_1} + C_2 e^{-t/\tau_2} + C_3 \qquad (2)$$

where C_1, C_2, and C_3 are constants, and τ_1 and τ_2 ($\tau_1 \ll \tau_2$) are the characteristic times corresponding to the early and later stages of coalescence.

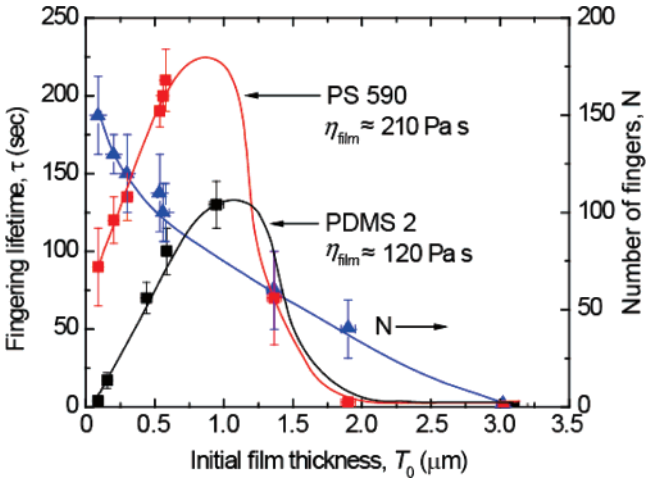

Figure 4. Lifetime of the transient fingering patterns τ and finger number N *vs* initial polymer film thickness T_0 for PS 590 ($\eta_{film} \approx$ 210 Pa s) and PDMS **2** ($\eta_{film} \approx$ 120 Pa s).

In the early stage, two surfaces jump into adhesive contact due to the van der Waals forces, and the contact area increases immediately on impact from zero to a finite radius reflecting the mainly elastic deformations of the substrate and polymer films. In the later stage, the growth is determined more by the viscous flow/drainage of the polymer.

II. Effect of Film Thickness. The lifetime τ of the transient fingering patterns is defined as the time from their appearance to their disappearance (when r_o and r_i merge). The growth of $2r_o$ and $2r_i$ of PS 590 for four different film thicknesses are shown in Figure 3. With increasing thickness, the τ first increases, then decreases, until finally—for films thicker than some critical value T_c—there is no obvious fingering pattern. Figure 4 shows a plot of τ *vs* T_0 for PS 590, showing a peak at $T_0 \approx 1$ μm. Films of various thickness were also tested with the other polymer melts, and were all found to exhibit similar trends. The results for PDMS **2** are also included in Figure 4.

III. Effect of Bulk and Thin Film Viscosity. As might be expected, the lifetime τ of the transient fingering instability was found to increase dramatically with the polymer's viscosity. First, the effective shear viscosities of the polymer thin films were obtained from SFA measurements of the shear forces between the surfaces as previously described,[29,45] and compared with the bulk values. Figure 5a shows two typical plots of the shear forces $F_{||}$ vs the shear velocities $V_{||}$ for PS 1390 films D = 260 nm thick at 60 °C, and PS 800 at D = 215 nm and 24 °C. The effective shear viscosity of the film, η_{film},was estimated using the following equation:[29]

$$\eta_{film} \approx \frac{5F_{||}}{16\pi RV_{||}\ln(2R/D)} \text{for } R \gg D \qquad (3)$$

Here R is the local radius of curvature, and D the closest distance of separation between the two curved surfaces during the shear measurements as shown in Figure 1. Table 1 compares the thin film and bulk shear viscosities of the six polymer samples investigated. We note that, within the measuring errors, the mean or effective viscosities are essentially the same as the bulk values for these submicrometer films, which should not be surprising, given that the films are all much thicker than R_g (see column 2 in Table 1). We should note, however, that the effective viscosities could be higher/lower near the surfaces and lower/higher near the centers of the films without affecting the mean values measured. Surface immobilization, wall-slip, shear alignment and entanglements could produce any of these effects.[52]

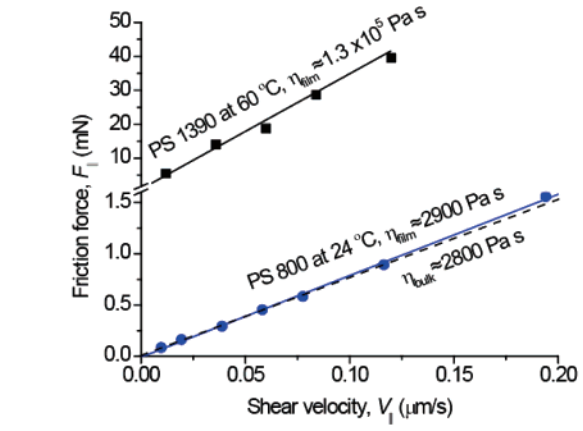

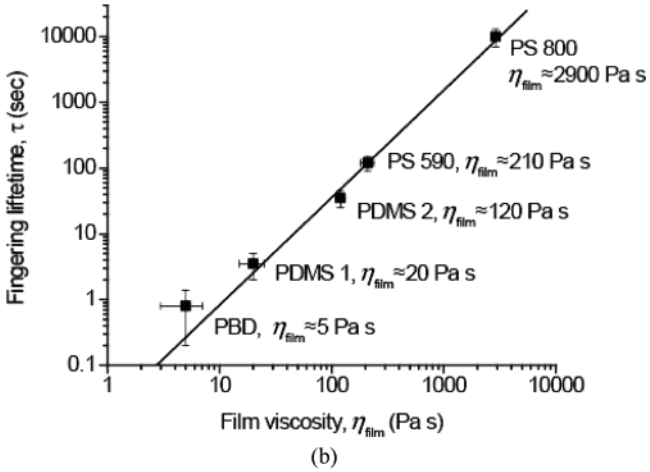

Figure 5. (a) Friction (shear) force vs shear velocities for PS 1390 at 60 °C (R = 2 cm, $D \approx$ 260 nm) and PS 800 at 24 °C (R = 2 cm, $D \approx$ 215 nm). (b) Effect of film viscosity on the lifetime of the transient fingering patterns for different polymers all having an initial film thickness T_0 of about 200 nm.

Figure 5b shows τ for different polymer melts with about the same thickness T_0 (around 200 nm) as a function of the film viscosity. The lifetimes were found to increase with the viscosities as

$$\tau \propto \eta_{film}^{\ n} \qquad (4)$$

with $n = 1.6 \pm 0.2$. For asymmetric systems (polymer melts spreading on a solid mica surface) we previously reported a value of $n = 2.1 \pm 0.2$.[46] The power law index for symmetric adhesion (coalescence) is a little smaller than for the asymmetric case.

To put things into a broader perspective, according to eq 4, for common (low viscosity) liquids such as water, alcohols and light oils (where η = 0.001−0.01 Pa s) these transient effects would be over within 1−100 μs. These very short times could be the reason why such effects have not been previously observed. Extrapolation of our results to fluid or soft particles and films, such as liquid and emulsion droplets, vesicles, and cells,[55,56] suggests that similar transient phenomena should exist during their interactions, which could be important for fully understanding the mechanisms of, for example, biological membrane fusion.

In the other limit of very high viscosity materials, such as highly viscoelastic polymers ($\eta = 10^3$−10^6 Pa s), pitch ($\eta \sim 10^7$ Pa s), and glaciers ($\eta \sim 10^{11}$ Pa s), rippled surfaces may also arise that change over very long or geological time scales.

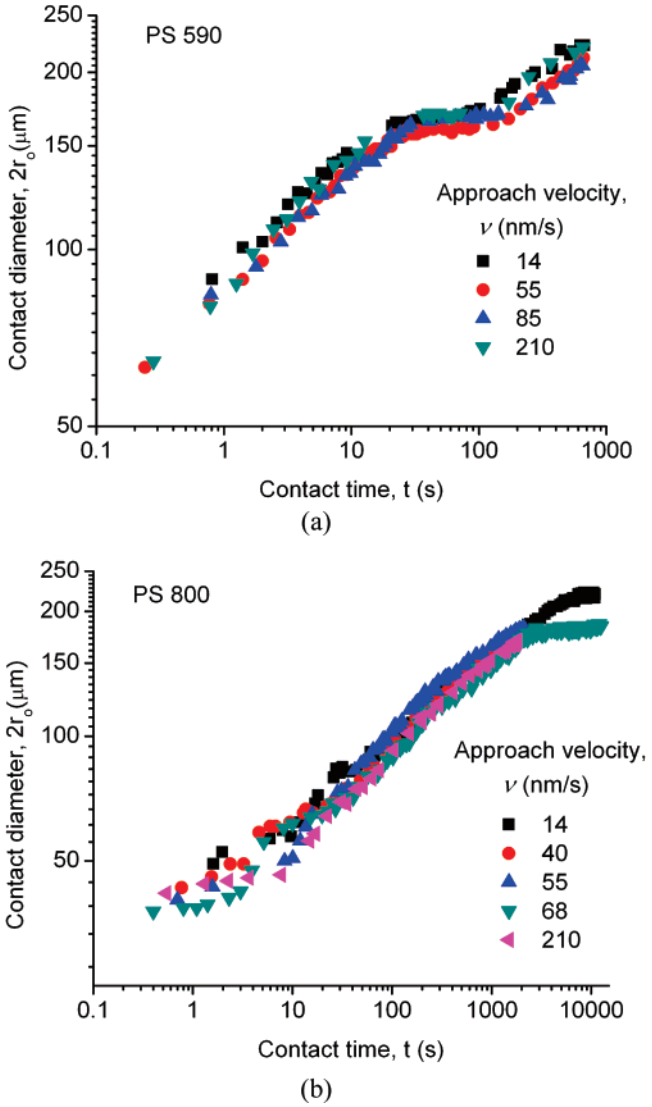

Figure 6. Effect of surface−surface approach rate on the rate of growth of the outer contact diameter, $2r_o$: (a) for PS 590; (b) for PS 800.

IV. Effect of the Approach Rate of the Surfaces. In order to establish the possible importance of the impact velocity on the incipient fingering patterns, different approaching rates were used to bring the two surfaces together. The growth of $2r_o$ with time for PS 590 and PS 800 are shown in Figure 6 for surfaces approaching contact at different approach rates, or velocities v, in the range 10−210 nm/s. The growth of both $2r_o$ (shown in Figure 6) and $2r_i$ (not shown) with time were found to be independent of v, which means that the approach rate of the two surfaces does not affect the appearance (and disappearance) of the transient fingering patterns. The probable reason for the velocity-independence of the fingering patterns is that the range of impact velocities in the experiments fell below the value at which the inertia of the colliding surfaces plays an important role during their coalescence.

We should note, however, that the actual impact velocity is higher than the approach velocity v due to the attractive van der Waals forces which accelerate the surfaces in the final stage (the last ~10 nm) of their coming into contact. It is interesting to calculate what the real impact velocity, v_i, actually is, which can be calculated as follows:

For two surfaces 1 and 2 in a geometry of two crossed cylinders having the same radius R approaching each other in a medium 3, the attractive van der Waals force is given by eq 5, and the critical jump-in distance D_J is given by eq 6, where D is the distance between the two curved surfaces, K is the force-measuring spring constant, and A_{132} is the Hamaker constant of the two surfaces 1 and 2 interacting across 3. A_{132} can be estimated using eq 7, where A_1, A_2, A_3 are the Hamaker constants of media 1, 2, and 3 in vacuum.

$$F_{vdW} = -\frac{A_{132}R}{6D^2} \tag{5}$$

$$D_J = \left(\frac{A_{132}R}{3K}\right)^{1/3} \tag{6}$$

$$A_{132} \approx (\sqrt{A_1} - \sqrt{A_3})(\sqrt{A_2} - \sqrt{A_3}) \tag{7}$$

The geometry of two crossed cylinders with the same radius R is locally equivalent to a sphere of radius R approaching a flat surface, and the equation of the motion during their approach can therefore be approximated by eq 8,

$$m\frac{d^2D}{dt^2} + \frac{6\pi R^2\eta_{eff}}{D}\frac{dD}{dt} = F_{vdW}(D) - K(D_J - D) \tag{8}$$

where m is the mass of the moving surface (which includes the polymer, mica, glue, and silica disk), and where the second term on the left is the hydrodynamic resistance to the approach of a sphere 1 to a flat 2 across a medium 3 with effective viscosity η_{eff}.[57]

An approximate solution to eq 8 that neglects the inertial term (first term on the left), the force due to the bending of the spring (second term on the right), and assumes a zero (or infinitely slow) external approach rate v, gives for the jump time from the critical separation D_J[57,58]

$$\tau_J = 18\pi R D_J^2 \eta_{eff}/A_{132} \tag{9}$$

and for the velocity at impact

$$v_i \approx \tau_J F_{vdW}(D_J)/m \tag{10}$$

In our experiments, two surfaces of the same polymer melts (medium 1 = medium 2) approach each other in air (medium 3). For polystyrene across air, $A_{132} = A_{131} \approx 6.6 \times 10^{-20}$J. For $K = 800$ N/m, $R = 0.02$ m, the calculated jump-in distance is $D_J \approx 8.2$ nm (cf. measured value of 9 nm). The mass of the moving surface m in our experiment is about 2 gram, and the viscosity of air is $\eta_{eff} = 1.8 \times 10^{-5}$ Pa s.[59] Substituting the above values into eqs 9 and 10 gives a jump-in time of $\tau_J = 20.6$ ms and an impact velocity of $v_i \approx 33\ \mu$m/s. Thus, the final impact velocity is much higher than any of the externally controlled approach velocities tested (typically less than 0.25 μm/s), which explains the absence of an effect (cf. Figure 6).

In a previous study,[45] we showed that fingering patterns of the type seen here are not due to inertial effects. In that study, two polymer films were brought into contact at $T < T_g$ and the temperature was then raised to $T > T_g$. Highly ordered fingers now appeared even though the adhesion involved no inertial effects. The importance of inertial forces for our system at high approach velocities was confirmed qualitatively in an experiment where the two surfaces were brought together fast, at approach rates ranging from 10 to 100 s of μm/s (i.e., greater than the calculated critical impact velocity of 30 μm/s). The lifetimes of the transient fingers were now much shorter and sometimes no fingers could be observed at all.

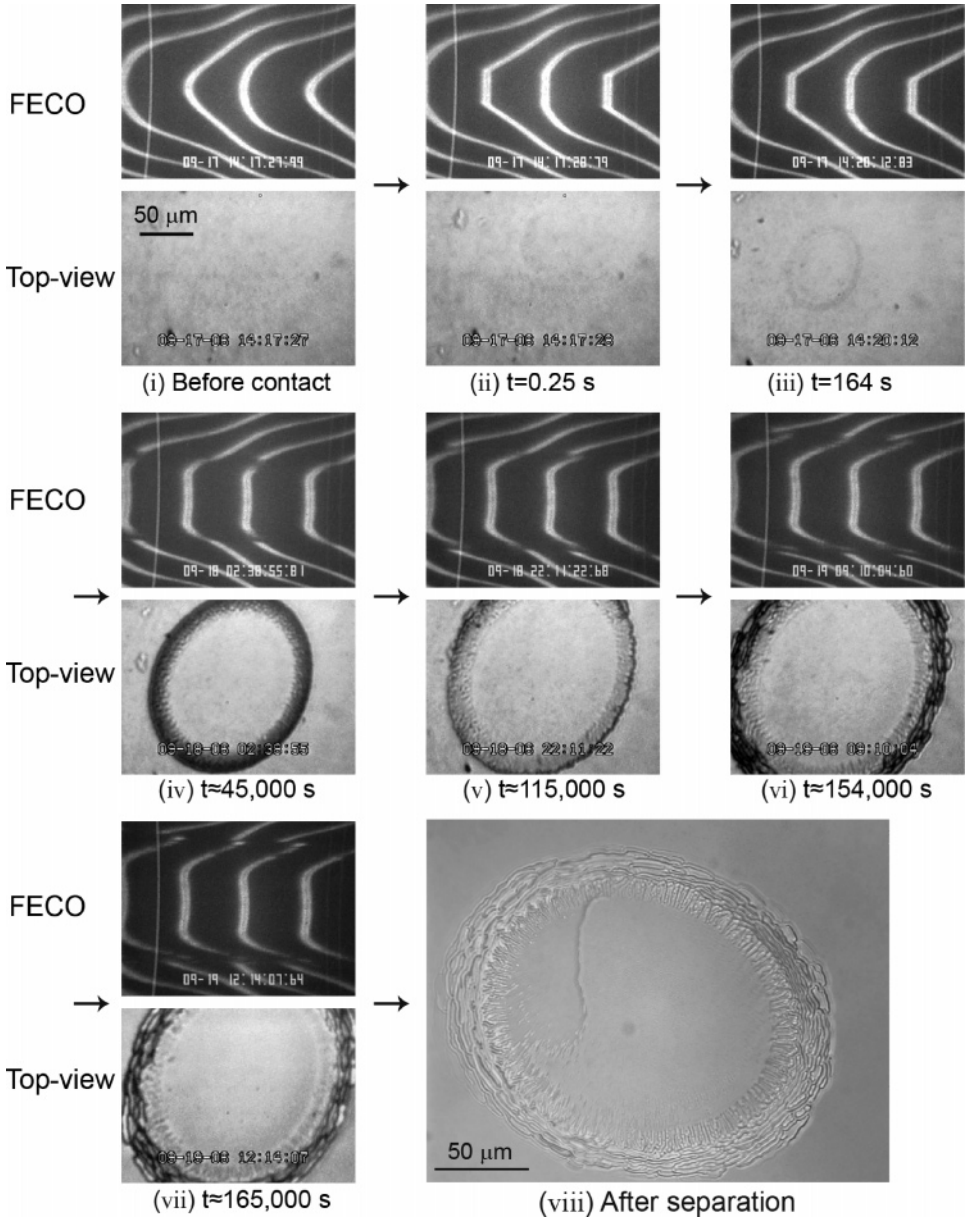

Figure 7. Time evolution of the fingering pattern of PS 1390 in the viscoelastic state (60 °C, initial film thickness $T_0 \approx 160$ nm): (i−vii) real time FECO and top-view microscopic images during the adhesive coalescence; (viii) microscopic image of a surface after freezing the structure using liquid N_2 and separating the two surfaces (using a Nikon OPTIPHOT 200 microscope).

The above analyses suggest (1) that impact velocities may often be determined by the local attractive forces rather than the externally driven motion and (2) that inertial effects do not play a role in the fingering or other patterns during coalescence of these systems at impact velocities below 30 μm/s. However, when the two surfaces approach each other at a rate greater than some critical impact velocity, the inertia of the surfaces does affect the resulting fingering pattern, whether transient or permanent. High inertia impacts of liquid drops on solid and liquid surfaces have been investigated for more than a hundred years: different impact patterns, such as neck distortions, radial jetting, and crown formation can occur depending on the impact speed, film thickness, fluid viscosity, surface tension, etc., which are of wide practical importance in coating and printing processes.[60]

V. Profiles of the Transient Fingering Patterns. The well-ordered fingers appear after the two surfaces jump into contact. Observation of the radially growing fingers shows that once they appear, the total number of fingers N does not change during the whole lifetime of the transient fingering pattern. Thus, their spacing increases with time. Defining the average spacing between two fingers as the finger wavelength λ, we may write $\lambda = 2\pi r/N = \pi(r_o + r_i)/N$, which in turn gives

$$\lambda \propto t^n \tag{11}$$

where $n = 0.2-0.3$, the same as that for the mean radius of the contact region.

The fingering number N was found to depend on the film thickness, decreasing with increasing T_0, as shown in Figure 4 (right-hand axis). Now, the initial wavelength immediately after the surfaces have come into flattened adhesive contact is, by definition, $\lambda_o = 2\pi a_o/N$,where a_o is the initial contact radius which, according to the JKR theory, is $a_o = (12\pi\gamma R^2/K)^{1/3}$, where γ is the surface energy (tension) of the contacting surfaces and K is effective elastic modulus of the system (a composite of the polymer film, mica, glue, and silica disk). The initial wavelength can therefore be expressed as

$$\lambda_o = 2\pi a_o/N = 2\pi(12\,\pi\,\gamma\,R^2/K)^{1/3}/N \tag{12}$$

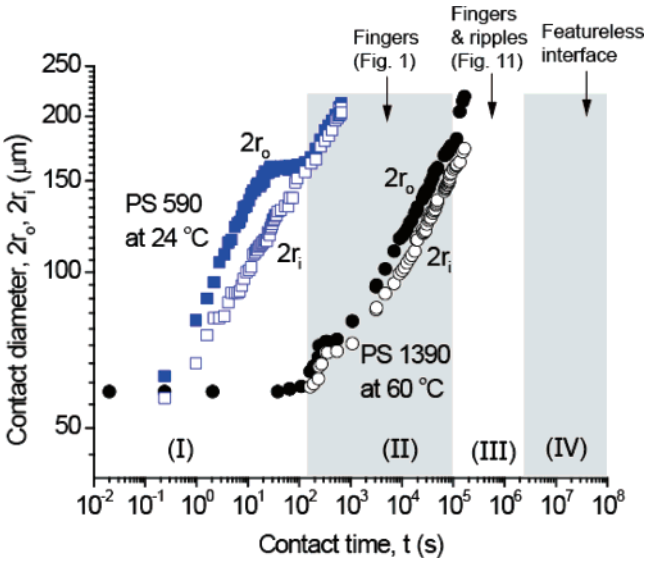

Figure 8. Time evolution of the fingering pattern of PS 1390 in the viscoelastic state (60 °C, initial film thickness $T_0 \approx 160$ nm): growth of the contact diameter vs time. The growth of the contact diameter vs time for PS 590 (24 °C, initial film thickness $T_0 \approx 101$ nm) is also shown for comparison.

For typical SFA experiments, the effective elastic modulus K of the composite material ranges from 10^{10} to 10^{12} Pa, depending on the thicknesses of the polymer, mica (Young's modulus $10^{11}-10^{12}$ Pa), glue layer (Young's modulus $\geq 2 \times 10^{10}$ Pa at 24 °C), and elastic/viscoelastic properties of the polymers.[10,59] Inputting the typical experimental values of $R = 2$ cm, $\gamma \approx 33$ mJ/m^2 (for polystyrene melts), and $K = 10^{10}-10^{11}$ Pa (as estimated above), the JKR part of eq 12 predicts $a_o = 17-37$ μm, which is close to typically measured values (cf. Figure 2), for example, $a_o = 17$ μm for $N \approx 150$, $a_o = 37$ μm for $N \approx 100$, and $\lambda_o = 0.7-2.3$ μm (in section VIII, we discuss the factors that determine λ_o and N).

For the same γ and R, the effective (composite) elastic modulus of the system K will decrease with increasing polymer thickness T_0 (since the polymers have a lower modulus than the substrates). Thus, a_o increases with increasing T_0. In contrast, the fingering number N was found to *decrease* with increasing T_0 (Figure 4), so from the above argument and eq 12, λ_o increases with the polymer film thickness T_0. However, once λ_o increases to the size of the contact radius r_o, no more fingers can appear, nor were any observed.

VI. Adhesive Contact and Surface Patterns in the Viscoelastic State. All the results and discussions so far have been for polymer melts in the "viscous state", i.e., with viscosities below about 3000 Pa s. More complex and interesting phenomena appear to arise for polymers in the viscoelastic state. (The viscoelastic properties of the six polymers used in these studies have been well studied and characterized,[61,62] but unfortunately the characteristic relaxation times of the specific molecular weights used at the shear rates and temperatures of the experiments are not known.) PS 1390 ($T_g \approx 46$ °C) was chosen for these studies; its viscosity can be changed from $\geq 10^{10}$ Pa s (glassy state) at 24 °C to 10^4-10^6 Pa s (viscoelastic state[61]) at 45−75 °C (cf. Figure 5a where 1.3×10^5 Pa s was measured at 60 °C).

Figure 7 shows images of the fingering patterns and the r *vs* time dependence of PS 1390 at 60 °C. In these experiments, the two PS 1390 films were mounted into the SFA chamber, which was then heated to 60 °C. After 5 h of film "equilibration" at this temperature the two surfaces were slowly brought

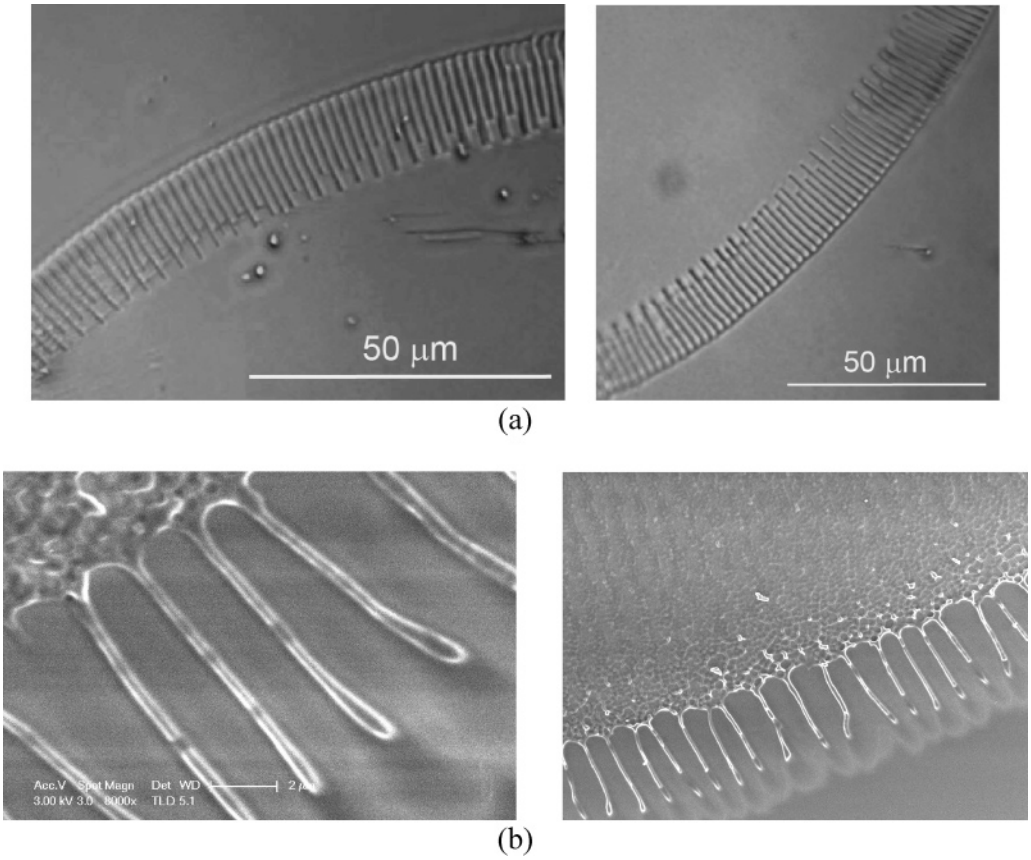

Figure 9. (a) Microscopic images of the frozen fractured finger patterns associated with adhesive coalescence of PS 1390 films at ~80 °C ($T_0 \approx 240$ nm). (b) SEM images of frozen fractured finger patterns from another experiment under similar experimental conditions.

toward each other (Figure 7i), jumping into flattened adhesive contact at $t = 0$ (Figure 7ii) due to the van der Waals force between them. The two surfaces were kept in contact for ~2 days (~2×10^5 s), during which real time FECO interference fringes and normal optical microscopic images were recorded simultaneously during the slow coalescence process (Figure 7).

The slowness of the coalescence allowed for detailed measurements to be made of the deformations in and around the adhesion zone which, in all likelihood, also occur for less viscous fluids, but much more rapidly. Immediately after the two surfaces jump into contact, Figure 7i→ii, a round, unrippled, contact boundary could be seen from the FECO and microscope images, as shown in Figure 7ii. This implies that during the initial (rapid) contact the two viscoelastic films behave elastically, producing a solid-like JKR contact, at least for polymers at temperature $T < T_g$, as has been reported before when De > 1.[49,50] After a few minutes, discontinuities at the contact edge can be observed on the even-order but not the odd-order FECO fringes (Figure 7iii), indicating that the discontinuities reflect local changes in the mean refractive index of the film but not its thickness.[29,43,44] Thus, the local geometry or profile of the polymer meniscus at the contact boundary is slowly changing due to local flow.

With increasing contact time, these deformations continue to grow into a fingering pattern (Figure 7, parts iv and v), which is very similar to that described earlier for the coalescence of viscous (or lower viscosity) polymers.[45] Figure 7vi shows that even after 40 h in contact, the fingering pattern is still growing outward. However, as also previously found for viscous fluids,[46] additional circular, concentric ripples or capillary waves now appear beyond the fingering pattern (i.e., at $r > r_o$), unlike the Saffman−Taylor fingers at $r < r_o$. Also, shown in Figures 1, 7, and 11, while the fingers point radially out from the center, the capillary waves or ripples are concentric circles. They arise from the perturbation of the local film thinning or "trough" outside of the contact region (just like the circular waves emanating from a perturbed liquid surface, for example, after a stone is thrown into a lake), and are therefore a bulk rather than a thin-film phenomenon. At $t = 46$ h, both the radial fingers and circular ripples coexist (Figure 7vii) and continued to persist for longer times. To further image these surface patterns, the contact region was quickly frozen or "quenched" with liquid nitrogen. The surfaces were then separated and both sides imaged using a normal optical microscope, shown in Figure 7viii.

Figure 8 shows the increasing pattern diameters with time. Assuming that eq 4 for the fingering llifetime, $\tau \propto \eta^n$, with $n = 1.6 \pm 0.2$, applies to PS 1390 at 60 °C, the lifetime for this polymer is predicted to be ~10^6 s (more than 12 days).

Our measurements suggest that, in general, coalescence can be divided into four distinct time regimes: (I) initial elastic (solid-like) contact where there is no time for flow, just an instantaneous elastic deformation of the fluid (and any supporting substrate surface), (II) radially growing fingers, (III) appearance of concentric ripples coexisting with the fingers, and (IV) disappearance of the ripples and fingers, leaving a smoothly continuous constant mean curvature surface. Figure 8 shows the first three of these regimes for PS 1390, where regime I is very short so that the contact diameter may be considered to be effectively constant (this regime being defined by the JKR-like shapes of the adhering surfaces). In regime II, the inner and outer contact radii increase as power law functions of time: $r_o \propto t^{0.16}$, and $r_i \propto t^{0.15}$; these power indices are slightly smaller than these for low viscosity liquids for which $n = 0.2-0.3$. However, these indices are very close to the theoretical prediction of $r \propto t^{1/7} = t^{0.14}$ for the growth of the contact radius with time during the sintering of two Maxwell viscoelastic spheres (particles) under zero load.[11,63]

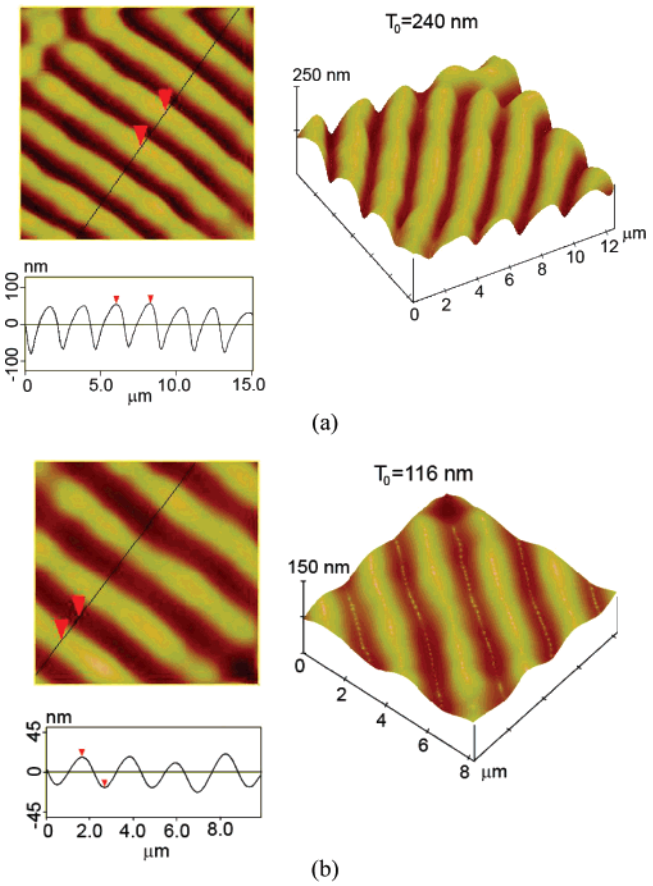

Figure 10. AFM images of the frozen fractured transient fingering patterns associated with adhesive coalescence of PS 1390 films at ~80 °C: (a) initial polymer thickness $T_0 \approx 240$ nm; (b) $T_0 \approx 116$ nm.

VII. Preservation of the Self-Organized Patterns for Imaging (and Possible Applications). The transient patterns associated with adhesive contacts were preserved as described at the end of the Materials and Experimental Methods. Figures 9 and 10 show typical SEM and AFM images in the "fingering" regime II of Figure 8. Each type of image provides further details on the highly ordered structure of the transient fingers, i.e., in addition to those obtained *in situ* during the experiments using FECO and optical microscopy (Figure 8). The fractured transient fingering patterns appear to be periodic waves with microscopic-scale periodicity (wavelength) but nanoscale "peak to valley" amplitude. Figure 10 shows a pattern for PS 1390 of initial thickness $T_0 \approx 240$ nm that developed a wavelength about 2 μm and an amplitude of about 100 nm; for thinner films of $T_0 \approx 116$ nm, the depth amplitude decreased to ~40 nm. The amplitudes of the waves were found to be approximately half of the thicknesses of the films for the range of thicknesses studied: 100−300 nm.

Preservation of such patterns can be achieved using a variety of methods, including cross-linking of the polymer chains, which may provide new ways to produce highly ordered patterned surfaces with potential technological and biomedical applications.

VIII. Mechanism of Transient Fingering Patterns. The appearance of the patterns and instabilities observed here during the adhesive contact of two symmetrical viscous or viscoelastic

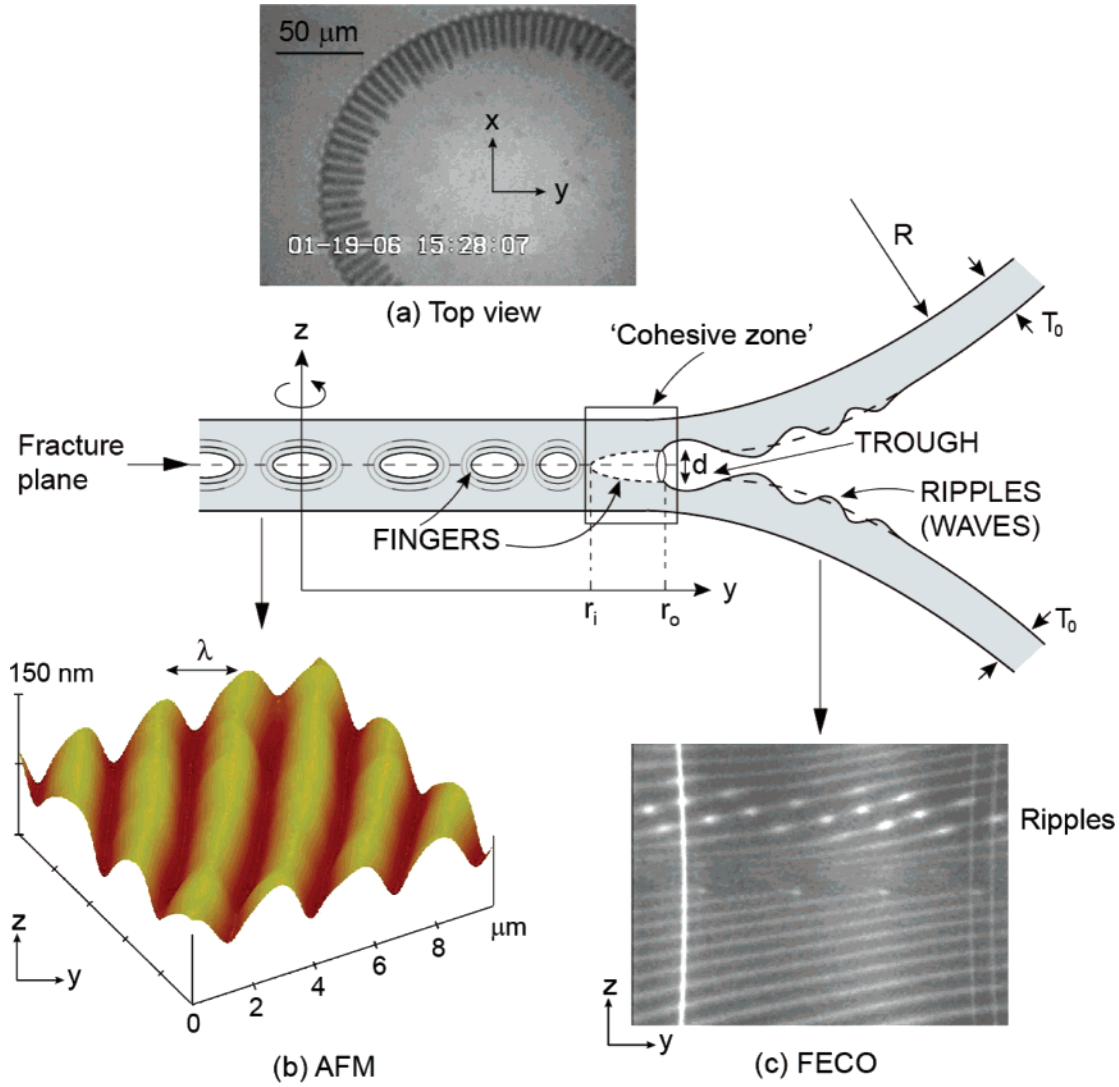

Figure 11. Schematics of the adhesive junction and "cohesive zone" in $x-y-z$ or $r-z$ coordinates and the corresponding typical experimental results. Key: (a) top view microscopic image of the transient radial fingering patterns in the $x-y$ plane; (b) three-dimensional AFM image of a finger pattern (frozen fractured in the fracture plane); (c) typical FECO fringe for the circular, concentric ripples, or waves propagating away from the contact region.

films is not expected from classic theories or models of either contact mechanics or "crack healing";[4,21,64] and we have previously shown[46] that these patterns are not due to the inertial impact forces when the two surfaces jump into contact. Regarding classic theories of contact mechanics,[1,8] these apply to elastic contacts in the static (equilibrium) state, while currently available viscoelastic models[11,15,19,26,64] do not give a complete picture of "contact dynamics", such as the time-evolution of a liquid or viscoelastic adhesive junction. Below, we propose an explanation for the observed phenomena based on theories of fluid mechanics and intermolecular and surface forces.

For most materials at a finite temperature, there is no clear boundary between the solid and liquid states: a material can behave like a solid or liquid depending on the time scale of the observation.[65] Thus, if two "solid" surfaces of the same material are kept in contact long enough, they will coalesce (completely mix) due to the thermal motion and flow of their atoms or molecules. In a previous report,[45,46] we proposed that the appearance of fingering patterns during the adhesion and coalescence of two fluid surfaces is due to the complex flow pattern that arises in this type of confined geometry (see Figure 1), where the driving force for flow is the high negative Laplace pressure generated at the highly curved concave meniscus at the rim of the (initially) circular neck. The development of radially tubular vapor fingers inside the growing meniscus (at $r \le r_o$) was attributed to the inward flow of fluid from outside the meniscus or contact radius ($r \ge r_o$), which is sucked in by the tensile Laplace pressure.

The removal of fluid from the region just outside the neck at $r \ge r_o$ causes the polymer film to thin at a velocity V_1 (cf. Figure 1). Now, in fluid mechanics, an interfacial fingering instabilitiy, known as the Saffman−Taylor instability, occurs whenever a fluid is displaced by a less viscous one−a theory that was originally developed to explain the "viscous fingering" observed in Hele−Shaw cells and porous medias.[66] Considering the global geometry of our experiment, the meniscus or neck radius keeps increasing as the spreading proceeds, driven by the high negative Laplace pressure generated at the highly curved *concave* meniscus at the rim of the contact junction. This pressure drags a large mount of polymer fluid into the growing neck, which in turn causes the (*convex* or *planar*) polymer film just outside the junction to thin, giving rise to a circular "trough" . As shown in Figure 1, in the region outside the neck, a *low*-viscosity fluid (air) displaces a *high*-viscosity fluid (polymer), thereby producing the conditions for generating Saffman−Taylor fingers−localized to the region near the meniscus rim at r_o. This local

effect is in contrast to the global situation where a high viscosity fluid (polymer) is displacing or pushing out a less viscous fluid (air) as the contact region expands. Theoretically, a Saffman−Taylor instability should generate a fingering pattern with wavelengths *greater than* some critical value, λ_c, given by[29,46,66]

$$\lambda_c \approx \pi b\sqrt{\frac{\gamma}{3V_1\eta}} \approx \pi b\sqrt{\frac{Rw(2r_o - w)\gamma}{3r_o^3V_2\eta}} \qquad (13)$$

where $V_1 \approx r_o^3V_2/Rw(2r_o - w)$ and $V_2 = dr_o/dt$, η is the viscosity of the polymer, γ its surface tension, R is the local radius of curvature, w is the width of the film-thinning region, and b is the gap distance between the two parallel plates in a Hele−Shaw cell type parallel-plate geometry. All of these parameters can be obtained from the experiments, as shown in Figures 1, 7a, 9, and 10 (from the AFM results of Figure 10, we can assume that $b \approx T_0/2$). Equation 13 has been shown to be consistent with the fingering wavelengths measured in similar experiments to those described here.[46] For $r_o \gg w$, as we have here (cf. Figure 1), eq 13 simplifies to

$$\lambda_c \approx \frac{\pi b}{r_o}\sqrt{\frac{2Rw\gamma}{3V_2\eta}} \qquad (14)$$

Recalling that the initial finger wavelength λ_o is related to the initial contact radius a_o and finger number N by eq 12, at the initial state, $r_o = a_o$, so λ_o depends on all the parameters in eq 14, where b, w, r_o ($= a_o$), and V_2 are mainly determined by the initial film thickness T_o, film viscosity η, and surface energy γ. Thus, λ_o is mainly determined by T_o, η, γ, and R. Using the following values from the experiment results: $r_o \approx 30$ μm, $w \approx r_o/10 \approx 3$ μm, and$V_2 \approx dr_o/dt \approx 7$ μm/s, for $\gamma = 33$ mN/m, $\eta = 230$ Pa s, and putting $b \approx T/2$, where T is the thickness of the polymer film (since b must be less than T), eq 14 yields $\lambda_c \approx 5$ μm for $T = 100$ nm, implying that viscous waves with wavelength greater than 5 μm are expected. For $\eta = 2800$ Pa s, we calculate $\lambda_c \approx 2$ μm. These values are consistent with the wavelength (periodicity) of the fingers observed in our systems.

Because of the perturbation (film thinning) at the trough region, additional *circular, concentric* ripples or "capillary waves" appear beyond the fingering pattern (i.e., at $r > r_o$), as shown in Figure 7vi−viii and Figure 11, which coexist with the finger patterns.

With time, as the neck volume and mean contact radius r_m grow, the Laplace pressure falls as does the fluid flow-rate. As the flow subsides, the fingering region diminishes, until the instabilities disappear and polymer−air interface is smooth.

Spontaneously growing bulges leading to fingers or other types of patterns can also be expected from a consideration of the different interaction forces that occur in the contact region just before and/or just after the two surfaces have come into adhesive contact. This region is sometimes referred to as the "crack-closure zone" or "cohesive zone" (Figure 11).

The proposed surface deformations are induced by a competition of the attractive van der Waals forces between the two surfaces (polymer−polymer or polymer−substrate[46]) which promote "bulging" or "curvature" and the effectively repulsive surface tension and elastic forces that oppose any change in the flat, zero curvature, geometry of the two opposing surfaces. The energy changes (per unit period of the fingers and per unit length parallel to the fingers, both in the $x-y$ plane) arising from these three forces, ΔE_{vdW}, ΔE_γ, and $\Delta E_{elastic}$ are given by eqs 15−18, where as shown in Figure 12, z is the separation

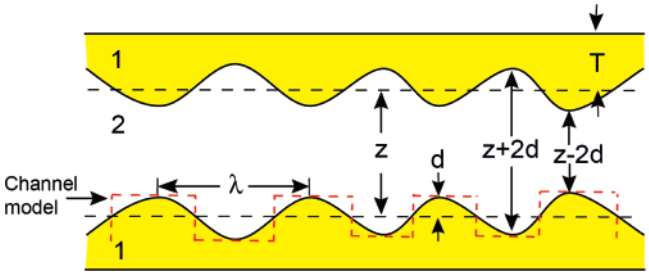

Figure 12. Schematic of two approaching and interacting surfaces 1 cross medium 2. z is the separation distance between the two undeformed surfaces, d is the amplitude of the surface perturbation (waves), λ is the wavelength (periodicity), and T is the film thickness.

distance between two undeformed surfaces, d is the amplitude of the surface perturbation (waves), λ is the wavelength (periodicity), T is the film thickness, E_{eff} is the effective elastic modulus for the composite system of the viscoelastic/viscous polymer film, mica, glue, and silica disk, and A_{121} is the Hamaker constant of the VDW interaction of two polymer surfaces 1 cross medium 2 (air).

$$\Delta E_{vdW} = -\frac{\lambda}{2}\cdot\frac{A_{121}}{12\pi}\cdot\left[\frac{1}{(z+2d)^2} + \frac{1}{(z-2d)^2} - \frac{2}{z^2}\right] \qquad (15)$$

$$\Delta E_{vdW} \approx -\frac{A_{121}d^2\lambda}{4\pi z^4} \qquad (16)$$

$$\Delta E_\gamma \approx 8d\gamma \qquad (17)$$

$$\Delta E_{elastic} \approx \frac{E_{eff}d^2}{T}\lambda \qquad (18)$$

The total energy change is given by eq 19. If $\Delta E_{total} \leq 0$, the attractive van der Waals force between the two surfaces (polymer−polymer or polymer−substrate) wins out, leading to eqs 20 and 21, showing that the instabilities will grow, resulting in periodic vapor fingers of wavelength λ once the bulges meet. The system is analogous to the "Rayleigh instability" that causes a cylindrical column of liquid to develop waves which eventually meet at the center resulting in a train of (unconnected) droplets.[3] Our 2D fingers are analogous to the vapor gap between these 3D droplets.

$$\Delta E_{total} = -\frac{A_{121}d^2\lambda}{4\pi z^4} + 8d\gamma + \frac{E_{eff}d^2}{T}\lambda \qquad (19)$$

$$\lambda \geq \frac{16\gamma}{d\left(\frac{A_{121}}{2\pi z^4} - \frac{2E_{eff}}{T}\right)} \qquad (20)$$

$$\frac{A_{121}}{2\pi z^4} \geq \frac{2E_{eff}}{T}, \quad \text{then } \lambda \geq 0 \qquad (21)$$

Inputting some typical values into eq 21, for polystyrene, $A_{121} \approx 6.6 \times 10^{-20}$ J, $T \approx 200$ nm, and $E_{eff} \approx 10^8$ Pa (upper bound), then $z \leq 2$ nm, while for $E_{eff} \approx 10^5$ Pa (lower bound), $z \leq 10$ nm, which implies that once the two surfaces are closer than 2−10 nm any surface undulations in the crack−closure zone should cause the wave crests on each surface to grow or "jump" into contact and form fingers. Also, inputting $z = 5$ nm, $d = z = 5$ nm, $E_{eff} \approx 10^5$ Pa, $A_{121} \approx 6.6 \times 10^{-20}$ J, $\gamma \approx 0.033$ J/m^2, and $T \approx 100$ nm into eq 20, we obtain $\lambda \geq 7$ μm, which is close to the observed wavelength. One should note that the effective elastic modulus E_{eff} in the above analysis may vary

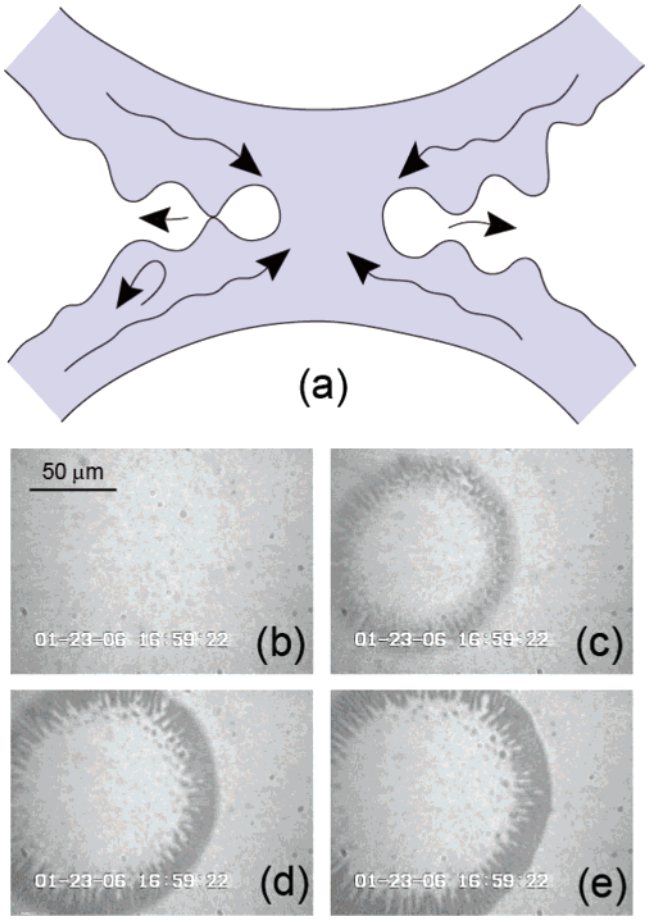

Figure 13. (a) Schematic of the early stages of the adhesive coalescence of two low-viscosity films. (b−e) Four continuous snapshots taken at 33 ms internals, during the adhesion of two PBD films ($\eta_{film} \approx 5$ Pa s, initial film thickness $T_0 \approx 260$ nm), contact occurred between parts b and c.

with the film thickness T, and the perturbation amplitude of the thin film d over any given time is also likely to depend on E_{eff} and T.

The fingers in this complex contact geometry cannot be considered to constitute the traditional *Maugis cohesive zone* which is a model describing the deformations in the nanoscale limit of a crack, i.e., at the bifurcation line. Thus, strictly, the traditional Maugis cohesive zone exists *inside* each finger. The cohesive zone here is more microscopic, describing the surface deformations over the whole contact region, as shown in Figure 11.

Figure 11a−c shows the schematics of the complex patterns observed inside and outside the adhesive junction and some corresponding typical experimental images, showing different views in $x-y-z$ planes. Figure 11a shows a top view microscopic image of a transient pattern of *radial* fingers in the $x-y$ plane; Figure 11b shows a three-dimensional AFM image of the same kind of pattern (an image of a frozen fracture plane); and Figure 11c is a typical FECO fringe pattern showing the *circular* ripples or capillary waves decaying and propagating away from the contact region due to the perturbation (film thinning) at the trough region.

For low viscosity fluids in the very early stage of fingering, there are some additional features besides the above analysis. Parts b−e of Figure 13 show four continuous snapshots (taken at 33 ms intervals) during the adhesion of two PBD films ($\eta \approx 6$ Pa s). Air bubbles can be seen to be trapped inside the contact zone, which coalesce with the growing fingers and disappear. The reason for the appearance and disappearance of the trapped bubbles is illustrated in Figure 13a. For low viscosity fluids, due to their rapid flow, the perturbation amplitude d_0 of the ripples/waves are so large that some of the crests on each surface coalescence. This can also be understood from eqs 20 and 21 which show that films of lower E_{eff}/T will have larger jump-in distances and larger amplitude waves and deformations. These bubbles, together with the initially less well-ordered waves outside the contact zone, rapidly develop into the well-ordered fingers observed, after which the above analysis for higher viscosity films applies.

The above analysis of the competing forces is similar to a recent analysis of permanent fingering patterns developed during the adhesion-driven crack closure of thin *purely* elastic solids.[37−40] However, in this analysis only the film thickness T appears to determine the wavelength λ of the fingers, given by $\lambda \approx \sqrt{2}\pi T$,[37] independent of the surface energy, velocity of the moving boundary, or material stiffness; whereas the fingering patterns observed with irreversibly flowing fluids depend on the surface energy, the velocity, and material viscosities. A rigorous theoretical treatment of the adhesion or contact dynamics of *viscoelastic* materials (especially thin films) has yet to be carried out, although theoretical studies on the adhesive contact and sintering of two Maxwell viscoelastic spheres are available[11,63,67] and, as concluded in section VI, predict the observed power-law index of the rate of growth of the fingers.

Conclusions and Perspectives

A new kind of transient fingering instabilities was found to generally exist associated with the adhesive contact and coalescence of polymers from the viscous to the viscoelastic states. The average contact radius was found to increase with contact time following $r = (r_i + r_o)/2 \propto t^n$, where n depends on the viscoelastic or viscous properties of the materials, with $n = 0.2-0.3$ for polymers with viscosities in the range $1-10^4$ Pa s, and $n \approx 0.15-0.16$ for polymers with viscosities of $\sim 10^5$ Pa s. The approach speed of the two surfaces was found to have no effect on the appearance of the transient fingering patterns when it is less than some critical value. The effects of polymer viscosity and film thickness on the lifetime of the transient fingers were studied in detail: the lifetime increases with the polymer viscosity as $\tau \propto \eta^n$, with $n = 1.6 \pm 0.2$. The lifetime peaks at some critical film thickness above which no transient fingers were observed. The wavelength of the finger patterns was found to increase with time as $\lambda \propto t^n$, where $n = 0.2-0.3$—essentially the same as the power index for the growth of the contact radius. The wavelength increases with the polymer film thickness. The wave number (number of fingers) N was found to remain constant during the whole lifetime of the transient fingering pattern, from its initial growth to its eventual disappearance, but N decreases (λ increases) with the polymer film thickness. The above scaling laws are summarized in The mechanism for the transient fingering patterns was discussed from two aspects: (1) fluid mechanics theories, and (2) intermolecular and surface forces, both of which can, apparently, explain the observed phenomenon.

Recent work has shown that fingering patterns can develop during the crack closure (adhesion) of thin elastic but soft polymers with elastic moduli of 10^5-10^6 Pa.[37−40] These patterns were reported to be *permanent*, not *transient*. However, following our observations that $\tau \propto \eta^n$, with $n = 1.6 \pm 0.2$ for symmetric (polymer−polymer) adhesion, and $n = 2.1 \pm 0.2$ for asymmetric (polymer−solid substrate) adhesion,[46] then for soft elastic materials with viscosities in the range 10^6-10^9 Pa

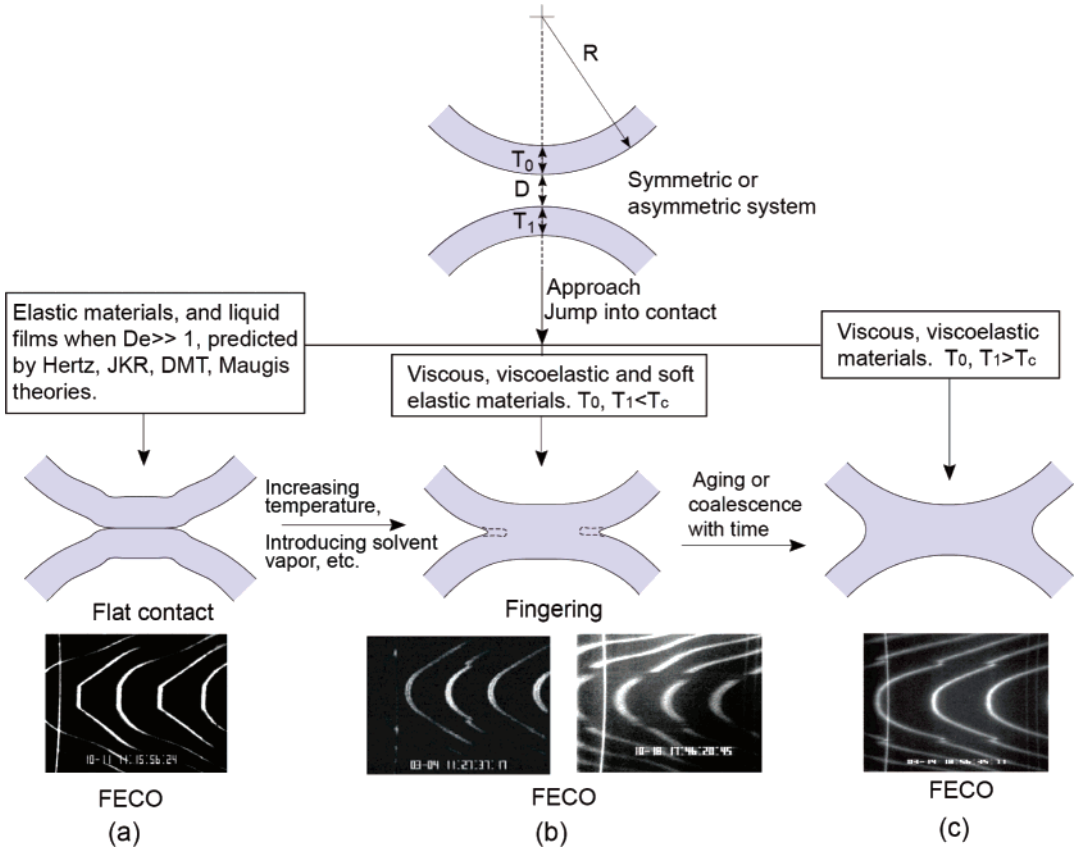

Figure 14. Schematics of the adhesive junctions of two films of different properties: (a) elastic films (with high elastic moduli) and liquid films when the Deborah number is high, De ≫ 1; (b) viscous, viscoelastic and soft elastic films (with low elastic moduli) of film thickness less than some critical value; (c) viscous and viscoelastic films (with low elastic moduli) of film thickness larger than some critical value.

s, the lifetimes of the fingering patterns would be expected to range from months to years, which may be the reason why the observed patterns appear to be permanent. Combining our present results with our previous studies,[45,46] overall, transient fingering patterns and instabilities can appear associated with three different kinds of adhesive contacts: (1) adhesion and coalescence (or spreading) of one surface on another *miscible* surface (for example, symmetric adhesion and coalescence of two similar materials); (2) adhesion or spreading of one surface on another fluid but *immiscible* surface; and (3) adhesion or spreading of one surface on another *solid* surface. These effects exist not only in polymeric systems but also in simple molecular systems (such as glucose).[68] Schematics summarizing the different types/stages of adhesion, spreading and coalescence are shown in Figure 14. For elastic materials (with high elastic moduli), their contact behavior can be predicted by classical theories of contact mechanics, such as the Hertz, JKR, DMT, and Maugis theories or models (Figure 14a). For viscous, viscoelastic, and soft elastic films (with low elastic moduli), transient fingering patterns and instabilities should occur but only if the films are thinner than some critical value (Figure 14b). For thicker films the lifetime of the transient fingering phenomena is too short, and no obvious fingering patterns were observed in the experiments (Figure 14c). Thus, transient fingers may not arise in the case of coalescing (bulk) spheres.

The highly ordered fingering patterns associated with adhesive contacts are "self-organized". These self-organized patterns can be preserved by using both physical and chemical methods such as quick quenching and UV cross-linking, which provides ways to produce patterned surfaces without using any external force, or field effects[69−73] and may have both scientific and technological importance in adhesion, wetting, lithography, microfluidics, and patterning applications. The transient fingering instabilities may also generally exist in biological surface interactions such as lipid vesicle−vesicle adhesion and coalescence, bilayer, and biomembrane interactions, cell−solid adhesion/binding, and cell−cell coalescence, which could be important to fully understand the mechanisms of these biological surface interactions.

Acknowledgment. This work was supported by the Materials Research and Science Engineering Center (MRSEC) Program of the National Science Foundation under Award No. DMR05-20415. Y. Tian thanks Tsinghua University for a Huaxin Distinguished Scientist Scholarship.

References and Notes

(1) Johnson, K. L. *Contact mechanics*; Cambridge University Press: Cambridge, U.K., and New York, 1985.
(2) Kendall, K. *Science* **1994**, *263*, 1720−1725.
(3) Israelachvili, J. N. *Intermolecular and surface forces*, 2nd ed.; Academic Press: Amsterdam and Boston, MA, 1992.
(4) Johnson, K. L.; Kendall, K.; Roberts, A. D. *Proc. R. Soc. London, Ser. A* **1971**, *324*, 301−313.
(5) Derjaguin, B. V.; Muller, V. M.; Toporov, Y. P. *J. Colloid Interface Sci.* **1975**, *53*, 314−326.
(6) Tabor, D. *J. Colloid Interface Sci.* **1977**, *58*, 2−13.
(7) Muller, V. M.; Yushchenko, V. S.; Derjaguin, B. V. *J. Colloid Interface Sci.* **1980**, *77*, 91−101.
(8) Maugis, D. *J. Colloid Interface Sci.* **1992**, *150*, 243−269.
(9) Dugdale, D. S. *J. Mech. Phys. Solids* **1960**, *8*, 100−104.
(10) Horn, R. G.; Israelachvili, J. N.; Pribac, F. *J. Colloid Interface Sci.* **1987**, *115*, 480−492.
(11) Hui, C. Y.; Baney, J. M.; Kramer, E. J. *Langmuir* **1998**, *14*, 6570−6578.
(12) Johnson, K. L. *Tribology Int.* **1998**, *31*, 413−418.
(13) Shull, K. R. *Mater. Sci. Eng. Rev.* **2002**, *36*, 1−45.
(14) Robbins, M. O.; Andelman, D.; Joanny, J. F. *Phys. Rev. A* **1991**, *43*, 4344−4354.

(15) Lin, Y. Y.; Hui, C. Y.; Baney, J. M. *J. Phys. D: Appl. Phys.* **1999**, *32*, 2250−2260.
(16) Cole, P. J.; Macosko, C. W. *J. Plastic Film Sheeting* **2000**, *16*, 213−222.
(17) Crosby, A. J.; Shull, K. R.; Lakrout, H.; Creton, C. *J. Appl. Phys.* **2000**, *88*, 2956−2966.
(18) Barthel, E.; Haiat, G. *Langmuir* **2002**, *18*, 9362−9370.
(19) Lin, Y. Y.; Hui, C. Y. *J. Polym. Sci., Part B: Polym. Phys.* **2002**, *40*, 772−793.
(20) Barthel, E.; Haiat, G. *J. Adhes.* **2004**, *80*, 1−19.
(21) Greenwood, J. A. *J. Phys. D: Appl. Phys.* **2004**, *37*, 2557−2569.
(22) Luan, B. Q.; Robbins, M. O. *Nature (London)* **2005**, *435*, 929−932.
(23) Greenwood, J. A.; Johnson, K. L. *J. Colloid Interface Sci.* **2006**, *296*, 284−291.
(24) Leger, L.; Joanny, J. F. *Rep. Prog. Phys.* **1992**, *55*, 431−486.
(25) Eggers, J.; Lister, J. R.; Stone, H. A. *J. Fluid Mech.* **1999**, *401*, 293−310.
(26) Maugis, D.; Barquins, M. *J. Phys. D: Appl. Phys.* **1978**, *11*, 1989−2023.
(27) Creton, C.; Kramer, E. J.; Brown, H. R.; Hui, C. Y. *Adv. Polym. Sci.* **2002**, *156*, 53−136.
(28) Falsafi, A.; Deprez, P.; Bates, F. S.; Tirrell, M. *J. Rheol.* **1997**, *41*, 1349−1364.
(29) Zeng, H. B.; Maeda, N.; Chen, N. H.; Tirrell, M.; Israelachvili, J. *Macromolecules* **2006**, *39*, 2350−2363.
(30) Shull, K. R.; Creton, C. *J. Polym. Sci., Part B: Polym. Phys.* **2004**, *42*, 4023−4043.
(31) Poivet, S.; Nallet, F.; Gay, C.; Teisseire, J.; Fabre, P. *Eur. Phys. J. E* **2004**, *15*, 97−116.
(32) Tirumkudulu, M.; Russel, W. B.; Huang, T. J. *Phys. Fluids* **2003**, *15*, 1588−1605.
(33) Derks, D.; Lindner, A.; Creton, C.; Bonn, D. *J. Appl. Phys.* **2003**, *93*, 1557−1566.
(34) Zeng, H. B.; Tirrell, M.; Israelachvili, J. *J. Adhes.* **2006**, *82*, 933−943.
(35) Gay, C.; Leibler, L. *Phys. Rev. Lett.* **1999**, *82*, 936−939.
(36) Mary, P.; Chateauminois, A.; Fretigny, C. *J. Phys. D: Appl. Phys.* **2006**, *39*, 3665−3673.
(37) Ghatak, A.; Chaudhury, M. K. *Langmuir* **2003**, *19*, 2621−2631.
(38) Shenoy, V.; Sharma, A. *Phys. Rev. Lett.* **2001**, *86*, 119−122.
(39) Monch, W.; Herminghaus, S. *Europhys. Lett.* **2001**, *53*, 525−531.
(40) Ghatak, A.; Chaudhury, M. K.; Shenoy, V.; Sharma, A. *Phys. Rev. Lett.* **2000**, *85*, 4329−4332.
(41) Adda-Bedia, M.; Mahadevan, L. *Proc. R. Soc. London, Ser. A* **2006**, *462*, 3233−3251.
(42) Chung, J. Y.; Kim, K. H.; Chaudhury, M. K.; Sarkar, J.; Sharma, A. *Eur. Phys. J. E* **2006**, *20*, 47−53.
(43) Israelachvili, J. *J. Colloid Interface Sci.* **1973**, *44*, 259−272.
(44) Israelachvili, J. *Nature Phys. Sci.* **1971**, *229*, 85.
(45) Zeng, H. B.; Zhao, B. X.; Tian, Y.; Tirrell, M.; Leal, L. G.; Israelachvili, J. *Soft Matter* **2007**, *3*, 88−93.
(46) Zeng, H. B.; Tian, Y.; Zhao, B. X.; Tirrell, M.; Israelachvili, J. *Langmuir* **2007**, *23*, 6126−6135.
(47) Israelachvili, J. N.; Mcguiggan, P. M. *J. Mater. Res.* **1990**, *5*, 2223−2231.
(48) Drummond, C.; Alcantar, N.; Israelachvili, J. *Phys. Rev. E* **2002**, *66*, 011705.
(49) Chen, N. H.; Maeda, N.; Tirrell, M.; Israelachvili, J. *Macromolecules* **2005**, *38*, 3491−3503.
(50) Maeda, N.; Chen, N. H.; Tirrell, M.; Israelachvili, J. N. *Science* **2002**, *297*, 379−382.
(51) DeGennes, P. G. *Rev. Mod. Phys.* **1985**, *57*, 827−863.
(52) McGuiggan, P. M.; Gee, M. L.; Yoshizawa, H.; Hirz, S. J.; Israelachvili, J. N. *Macromolecules* **2007**, *40*, 2126−2133.
(53) Luengo, G.; Schmitt, F. J.; Hill, R.; Israelachvili, J. *Macromolecules* **1997**, *30*, 2482−2494.
(54) Horn, R. G.; Israelachvili, J. N. *Macromolecules* **1988**, *21*, 2836−2841.
(55) Helm, C. A.; Israelachvili, J. N.; Mcguiggan, P. M. *Science* **1989**, *246*, 919−922.
(56) Chiruvolu, S.; Walker, S.; Israelachvili, J.; Schmitt, F. J.; Leckband, D.; Zasadzinski, J. A. *Science* **1994**, *264*, 1753−1756.
(57) Raviv, U.; Laurat, P.; Klein, J. *Nature (London)* **2001**, *413*, 51−54.
(58) Benz, M.; Chen, N. H.; Jay, G.; Israelachvili, J. I. *Ann. Biomed. Eng.* **2005**, *33*, 39−51.
(59) Lide, D. R. *CRC handbook of chemistry and physics*, 86th ed.; CRC Press: Boca Raton, FL, 2005.
(60) Rein, M. *Fluid Dyn. Res.* **1993**, *12*, 61−93.
(61) Ferry, J. *Viscoelastic properties of polymers*, 3rd ed.; Wiley: New York, 1980.
(62) Santangelo, P. G.; Roland, C. M. *Macromolecules* **1998**, *31*, 4581−4585.
(63) Lin, Y. Y.; Hui, C. Y.; Jagota, A. *J. Colloid Interface Sci.* **2001**, *237*, 267−282.
(64) Greenwood, J. A.; Johnson, K. L. *Philos. Mag. A* **1981**, *43*, 697−711.
(65) Larson, R. G. *The structure and rheology of complex fluids*; Oxford University Press: New York, 1999.
(66) Saffman, P. G.; Taylor, G. *Proc. R. Soc. London Ser. A* **1958**, *245*, 312.
(67) Jagota, A.; Argento, C.; Mazur, S. *J. Appl. Phys.* **1998**, *83*, 250−259.
(68) Zhao, B. X.; Zeng, H. B.; Tian, Y.; Israelachvili, J. *P. Natl. Acad. Sci. U.S.A.* **2006**, *103*, 19624−19629.
(69) Tsori, Y.; Tournilhac, F.; Leibler, L. *Nature (London)* **2004**, *430*, 544−547.
(70) Schaffer, E.; Thurn-Albrecht, T.; Russell, T. P.; Steiner, U. *Nature (London)* **2000**, *403*, 874−877.
(71) Wu, N.; Pease, L. F.; Russel, W. B. *Adv. Funct. Mater.* **2006**, *16*, 1992−1999.
(72) Wu, N.; Russel, W. B. *Appl. Phys. Lett.* **2005**, *86*, 241912.
(73) Zeng, H. B.; Tian, Y.; Anderson, T. H.; Tirrell, M.; Israelachvili, J. N. *Langmuir* 2007, DOI: 10.1021/1a7017242.

MA0712807